Numerical Modeling of Shear Stress and Displacement Reversals as a Pit Floor Passes a High Wall and Implications for Progressive Shear Strength Degradation

Navid Bahrani
Geomechanics Research Centre, MIRARCO - Mining Innovation, Laurentian University, Sudbury, ON, Canada

Dwayne D. Tannant
School of Engineering, The University of British Columbia - Okanagan, Kelowna, BC, Canada

ABSTRACT: Evidence of elastic rebound around natural valleys or artificial surface excavations has been documented in the literature. Rock excavation alters the initial state of stress adjacent to the excavation. This unloading process can reduce the rock mass strength near the excavation. Few examples in the literature have examined the influence of unloading and elastic rebound on the strength degradation of the remaining rock mass around surface excavations. In this study, a finite element program was used to assess the effect of excavation unloading and the consequent elastic rebound on progressive shear strength degradation of bedding surfaces. For this purpose, a hypothetical planar footwall slab was modeled with different excavation stages and pit depths. A joint boundary consisting of 30 joint elements was used to simulate the slip surface. The distributions of shear stress and displacement along the joint, current and cumulative numbers of yielded joint elements, and the global factors of safety for slab slip were compared and validated with limit equilibrium analyses. It was demonstrated that shear stress and displacement reversals occur along the slip surface as the slab is being passed by the pit floor. The modeling results provided insight into progressive shear strength degradation that occurs when the pit floor approaches and passes a specific point in the highwall.

1 INTRODUCTION

Surface coal mines in mountainous terrain are susceptible to footwall slope instabilities. The stability of footwall slopes is mainly controlled by the height and steepness of the slopes and the orientation of structural features such as faults, shears, and rolls relative to the slope face. The common failure modes identified in footwall slopes are planar, bilinear, buckling, and ploughing failures. The stability analyses of these footwalls have been traditionally carried out using two-dimensional limit equilibrium techniques. The application of numerical modeling techniques for the analysis of the footwall failure modes has recently become popular (Stead & Eberhardt 1997). The advantages of numerical modeling over limit equilibrium analysis in geotechnical engineering practice have been documented in the literature. As stated by Krahn (2003), the fundamental shortcoming of limit equilibrium methods, which only satisfy equations of statics, is that they do not consider strain and displacement compatibility, which has two serious consequences: local variations in factors of safety along the slip surface cannot be considered and the computed stress distributions are often unrealistic. The important capability of numerical modeling in simulating the history of the mining operation has not been widely adopted by researchers and engineers. In most cases, the modeling of excavation history is conducted to mainly back-analyze the state of *in situ* stresses from deformations measured in the field or to simulate the failure mode.

Simulation of the excavation history makes it possible to understand progressive strength degradation of the remaining rock mass around an excavation. While this notion has widely been used for underground openings, little work has been done to simulate rock mass strength degradation around surface structures such as open pits, and little attempt has been made to evaluate the effects of excavation unloading and the consequent elastic rebound on the shear strength degradation of bedding surfaces that are typically found in footwall slopes.

The removal of a volume of rock from either surface or underground changes the initial state of stress adjacent to the excavation. The stresses perpendicular to the excavation surface decrease. This unloading process can reduce the strength of the rock mass near the excavation. The zone of influence, which is known as the excavation damaged zone in the literature, increases with the scale of the project. Hence, the excavation-damaged zone is often larger for surface excavations than in underground excavations. Goodman and Kieffer (2000) also noted that surface excavations generally tend to be less stable than underground excavations.

Matheson and Thomson (1973), based on the results of air photo surveys along rivers in central Alberta, suggested that elastic rebound due to vertical stress relief caused by valley erosion is the mechanism that produced features such as raised valley rims, sloughs parallel to the valley crest, and upwarping of the beds that will locally influence the dip of the bedrock. Imrie (1991) reported other rebound features caused by valley down cutting by the Peace River at three dam sites in British Columbia. It was stated that valley erosion resulted in upward arching of the central valley floor accompanied by horizontal bedding plane fractures as well as tensile vertical fractures called the hinge zone, and inward movement of the valley walls, which produced vertical relaxation joints. The 150 m deep excavations of ship locks associated with the Three Gorges Dam in China prompted a comprehensive investigation including field testing and monitoring, numerical modeling, and back analysis by Deng et al. (2001) and Sheng et al. (2002). Analysis of the ship lock excavations noted the presence of extensive disturbed zones caused by rebounding deformation due to the unloading process as well as blasting operations. Eberhardt et al. (2003) indicated that the discontinuities that contributed to the initiation, development, and occurrence of the 1991 Randa rock slope failure were sub-parallel to topography. They further explained that these joints are stress-relief or sheet joints and are accepted to be the result of rock dilation due to unloading effects caused by glacial erosion processes. Using 2D finite element numerical modeling, Panthi and Nilsen (2006) demonstrated that unloading due to large massive rock slope failure increases the probability of further collapses. Modeling results have shown that the unloading caused by the 1934 Tafjord slide has increased the stress anisotropy as well as the displacements near the top of the slope that may cause the development of new tensional joints, which in turn increase the potential for instability of the new slope geometry.

Surface unloading either naturally (erosion, glacial retreat and large slope failure) or man-made (open pit) and its associated ground rebounding can deteriorate the strength of the remaining rock mass, which increases the potential of future surface failures. In these examples, most of the research was directed to the final stage of the unloading process where the slope of interest is fully exposed. The notion of shear strength degradation of bedding surfaces during the process of unloading when the valley bottom approaches and passes a certain point near the slope profile on a bedding surface is not widely recognized.

This paper deals with modeling the behaviour of footwall slopes and associated excavation-dependent progressive shear strength degradation or damage to bedding surfaces. The results of a series of numerical analysis of a generic footwall slab that is exposed by mining in a series of stages are presented. For this purpose, the finite element program Phase2 (Rocscience 2007) was used. The modeling results provided new insight into progressive shear strength degradation that occurs when the pit floor approaches and passes a specific point in the highwall.

2 NUMERICAL MODELS

2.1 *Pit geometries and excavation stages*

For the purpose of simulating the unloading process in a generic open pit mine, three cases with different model geometries were developed. Each case simulates the geometry of a 25 m high bench face at slope of 60º at the bottom of a pit. Each model consists of a planar slab with a length of 8 m and a thickness of 1 m, located on the lowest slope of the pit. An elastic-perfectly plastic joint boundary parallel to the slope face was used to simulate a bedding surface along which the slab is given freedom to slide. Figure 1 shows the geometry of Phase2 models developed for Cases 1 to 3. To minimize the boundary effects on modeling results, the boundary geometries were selected so that the depth and width of each model are respectively two and four times the depth of pit floor.

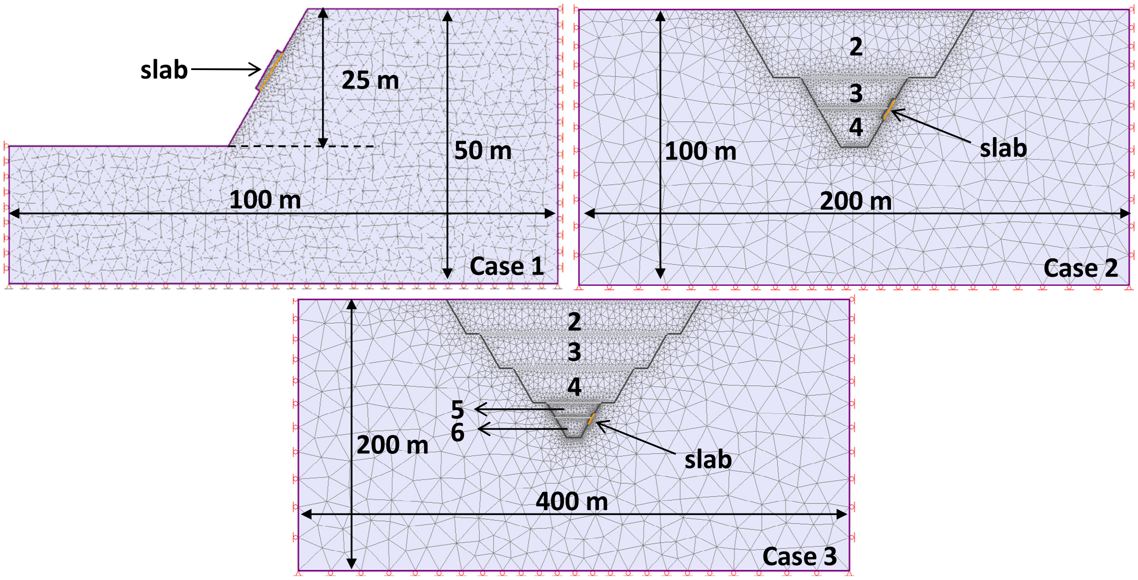

Figure 1 Three Phase2 models showing geometries and mesh discretization

Case 1 simulates only the last stage of a pit bottom with no previous excavations present in the model. Cases 2 and 3 consist of multiple excavation stages to capture the progressive development of a pit from a horizontal ground surface down to the pit bottom. The first stage in these two cases represents the application of the *in situ* stresses with a horizontal ground surface. All displacements in the model were set to zero at stage 1. Excavations start from stage 2. Stage 2 in Case 2 and stages 2, 3 and 4 in Case 3 represent the excavation of a full slope height. The last two stages in these two cases include the excavation of the first half of the slope height where the upper half of the slab is first exposed following by the excavation of the second half of the slope height in the last stage where the final pit floor is excavated, the slab is fully undercut, and the slab can freely slide.

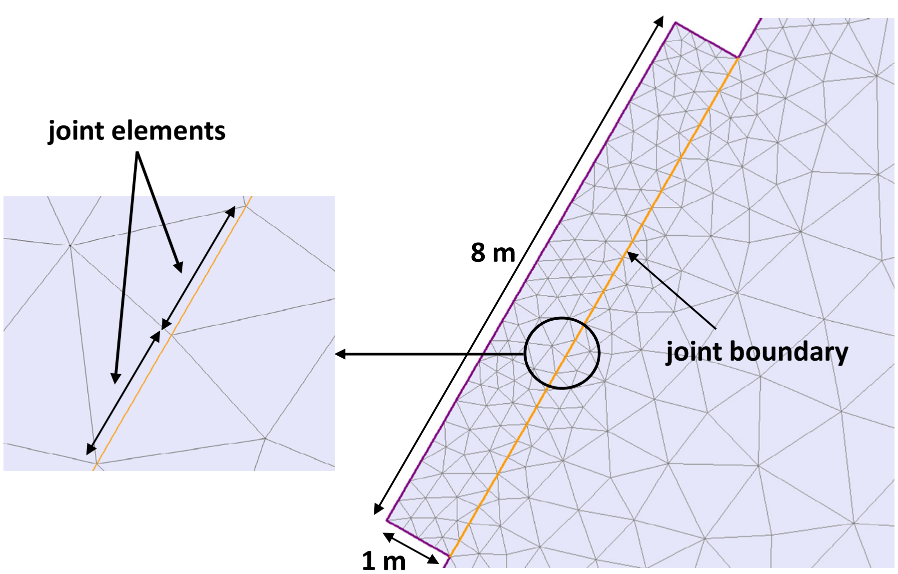

Figure 2 Slab geometry and joint boundary discretized into 30 joint elements

Phase2 has an automatic mesh generation scheme. To produce results in acceptable time, all the finite element models that are discussed in this study were constructed with 3-noded triangular elements and a graded mesh. All models used the same convergence parameters including 500 iterations and a tolerance of 0.001. The initial number of nodes on external boundaries was selected to be 200. To capture more accurate results, the mesh discretization as well as mesh density were increased around the slab and the pit bottom. The total number of elements and nodes were respectively 2347 and 1295 for Case 1, 4378 and 2300 for Case 2 and 5272 and 2745 for Case 3.

2.2 *Geotechnical properties*

To keep the numerical analysis simple, only one rock type was used in all cases. The rock was modeled as an isotropic elastic medium. Table 1 list the hypothetical rock and discontinuity properties selected as inputs in the numerical models.

Table 1 Rock mass and discontinuity properties used in the numerical models

Rock mass			Joint			
Young's modulus	Poisson's ratio	Density	Cohesion	Friction angle	Normal stiffness	Shear stiffness
MPa		g/cm^3	MPa		MPa/m	MPa/m
20000	0.3	2.7	0.05	25º	10000	1000

Joint boundaries consisting of 30 joint elements as shown in Figure 2 were used to model the presence of a planar bedding surface at the base of the exposed footwall block. A joint boundary in a Phase2 analysis can be allowed to slip by choosing a joint slip criterion. Phase2 analyses that included joint slip used a Mohr-Coulomb failure criterion for joints.

The initial horizontal/vertical stress ratio is required for a Phase2 model. The vertical stress was assumed equivalent to the weight of overlying rock mass. In rock, the maximum horizontal stress is often greater that vertical stress at relatively shallow depths (Sheorey 1994). However, the preliminary analyses were carried out with the in-plane stress ratio of unity. Further analyses were then conducted with the ratio of maximum horizontal stress to vertical stress (in-plane stress ratio) of 2 and 3.

3 EFFECT OF UNLOADING AND EXCAVATION DEPTH

The effects of the unloading process and depth of excavation on stresses, displacements, and stability along the joint were assessed. The results obtained from this process (Cases 2 and 3) including changes in the magnitudes and directions of shear stresses and displacements as well as the stability of the slab are compared with those obtained from Case 1 where the slab is in the condition of sliding under its self-weight.

Figure 3 shows the distributions of shear stress along the joint in Case 1 and in the last stage of Cases 2 and 3 when the final pit floor is excavated. Note that the 'distance along joint' goes from zero at the top of the slab to 8 m at the bottom of the slab for all figures in this paper. This figure reveals that in Case 1, where the slab is free to slide under self-weight, the sense of shear is positive with its magnitude approximately constant throughout the joint. However, in Cases 2 and 3, the sense of shear along the upper half of the joint is positive (downward slab motion) followed by a sudden drop to negative stresses in the middle of the slab at the point where the pit floor was reached in the stage before the final stage (stage 3 in Case 2, and stage 5 in Case 3). In the lower part of the slab, the shear stresses gradually rise to zero and then to positive values. This shows that the rebound caused by the unloading process due to pit excavation results in reversal in the sense of the shear stresses acting along bedding surface. This phenomenon, which is called "shear stress reversal", is discussed in more detail in the following sections.

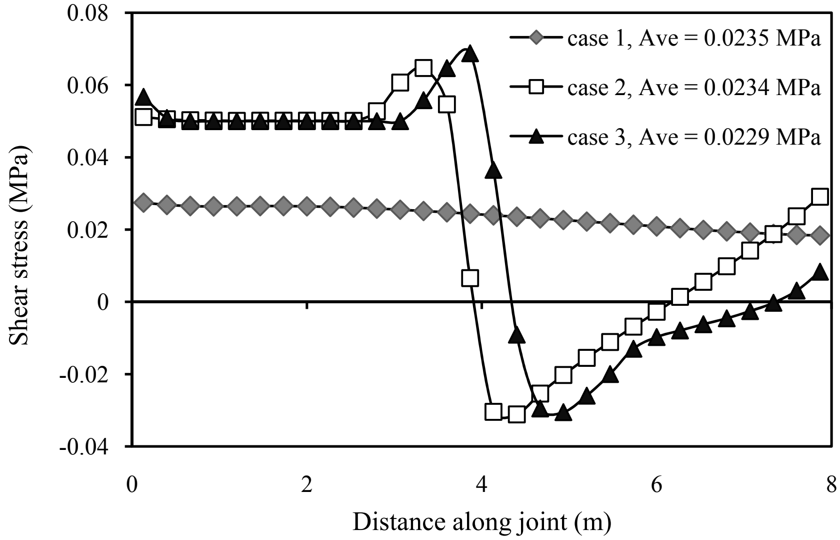

Figure 3 Shear stress along the joint in Case 1 and final stage of Cases 2 and 3

Figure 4 shows that shear displacements along the joint in Case 1 are positive indicating downward slab sliding. However, in Case 2 shear displacements along the upper part of the slab are negative. Only a small portion of the joint in the lower part has positive shear displacements. In Case 3, where the final pit floor is two times deeper than in Case 2, the shear displacement throughout the joint is negative indicating the upward movement of the whole slab. This behaviour along the joint or a bedding surface, observed in Cases 2 and 3, is believed to be a consequence of valley rebound. As the pit floor progresses to deeper levels, the effect of elastic rebound becomes more important and causes greater upward movement as seen in differences between Cases 2 and 3.

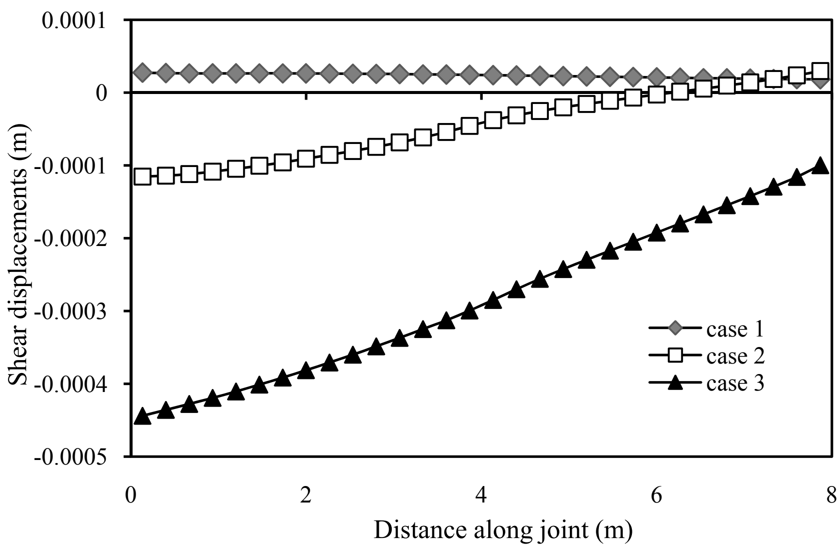

Figure 4 Joint shear displacements for Case 1 and final stage of Cases 2 and 3

More analyses were carried out to understand the influence of the excavation depth and unloading on the stability (factor of safety) of the footwall slab by comparing the results obtained from different cases with those from the conventional limit equilibrium calculations. The stability analysis of a simple planar slab by using conventional limit equilibrium technique can be done assuming a simple planar failure mechanism with no water pressure, in which case the factor of safety *FS* is given by (Hoek & Bray 1981):

$$F = \frac{cA + W\cos\theta\tan\phi}{W\sin\theta} \tag{1}$$

In this equation, W is the weight of the slab, θ is the dip of the slip surface of area A, and c and ϕ are the Mohr-Coulomb strength parameters for the slip surface. Using this method, the factor of safety of the slab with no support force was calculated to be 2.45.

A factor of safety for slab slip obtained from a Phase2 analysis is needed for comparison with limit equilibrium analysis. The global factor of safety for slab slip is simply obtained by dividing the average of shear strength by the average of shear stresses acting along the joint boundary as shown in Equation 2.

$$FS = \frac{\tau_{ave}}{(\tau_f)_{ave}} = \frac{c + (\sigma_n)_{ave}\tan\phi}{(\tau_f)_{ave}} = \frac{c + \left(\left[\sum_{i=1}^{m}(\sigma_n)_i\right]\Big/m\right)\tan\phi}{\left(\sum_{i=1}^{m}(\tau_f)_i\right)\Big/m} \tag{2}$$

In Equation 2, τ_{ave} and $(\tau_f)_{ave}$ are respectively the average shear strength and shear stress along the joint boundary. The shear strength of the joint can be calculated using the Mohr-Coulomb failure criterion where c and ϕ are 0.05 MPa and 25º, respectively, for each element. Since the joint boundaries in all the Phase2 models were discretized into 30 joint elements of equal length (i = 1 to 30, m = 30), the average shear strength and shear stress along the joint can be obtained by simply averaging respective normal (σ_n) and shear (τ_f) stresses obtained from the joint elements. The limit equilibrium factor of safety and the finite element global factors of safety for slab slip are compared in Figure 5.

Figure 5 reveals that although the distributions of shear stress and normal stress along the joint for each case are different, the global factors of safety for slab slip in Case 1 and in the last stages of Cases 2 and 3, obtained using Equation 2, are almost the same and very close to that of a simple limit equilibrium analysis. The reason is that the average shear and normal stresses acting along the joint, which are the required parameters in Equation 2, are very close in magnitudes for each case (23 kPa and 14 kPa, respectively).

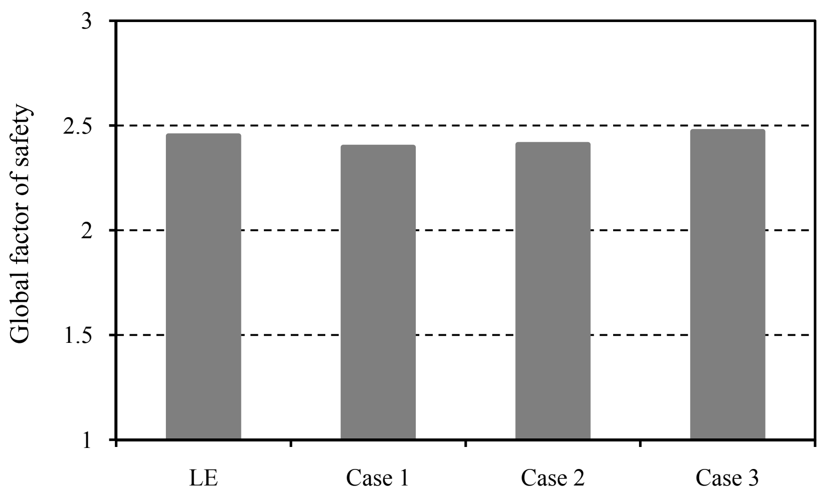

Figure 5 Comparison between FE factors of safety in Case 1 and in the last stage of Cases 2 and 3 and LE factor of safety

As mentioned earlier the joint was discretized into 30 elements with equal length. To understand better the effect of unloading process and the consequent elastic rebound on the slab response, the number of yielded joint elements was obtained from Case 1 and the last stage of Cases 2 and 3. For Case 1, none of the joint elements yielded, however in the last stages of Case 2 and Case 3, 25 and all 30 joint elements yielded, respectively. This indicates that excavation unloading causes overstressing on the bedding plane forming the base of the slab. Moreover, as the pit depth increases the rebound phenomenon and the consequent overstressing becomes more dominant leading to increased yielding along the bedding plane. A question may arises here concerning how the global factor of safety can be much bigger that 1.0 yet yielding has occured everywhere in the last stage of Case 3. The answer to this question will be discussed in the following sections.

4 MODELING SHEAR STRESS AND DISPLACEMENT REVERSALS AND EXCAVATION-DEPENDENT DAMAGE ALONG BEDDING SURFACES

The notion of stress rotation due to the advancement of a tunnel face has been documented in the literature (Kaiser et al. 2000, Eberhardt 2001, Diederichs et al. 2004). It is now understood that this phenomenon has influence on rock mass degradation (damage) around underground openings. As explained earlier and shown in Figure 3, a change in the sense of shear stress along the joint in models simulating the valley rebound was observed.

To understand better the effect of unloading on this phenomenon, modeling of Case 2 was carried out with multiple excavation stages that progressively exposed the slab. Stage 1 in this model simulates the development of the original ground surface. All the displacements were set to zero at this stage. Stages 2 and 3 represent the excavation of the rock mass above the slab. Stages 4, 5, 6 and 7 simulate the process of down-cutting of the pit floor along the slab. In the last two stages (stages 8 and 9), the slab is fully exposed and free to slide along the joint boundary according to the Mohr-Coulomb strength parameters. Figure 6 displays the locations of the pit floor at stage 7.

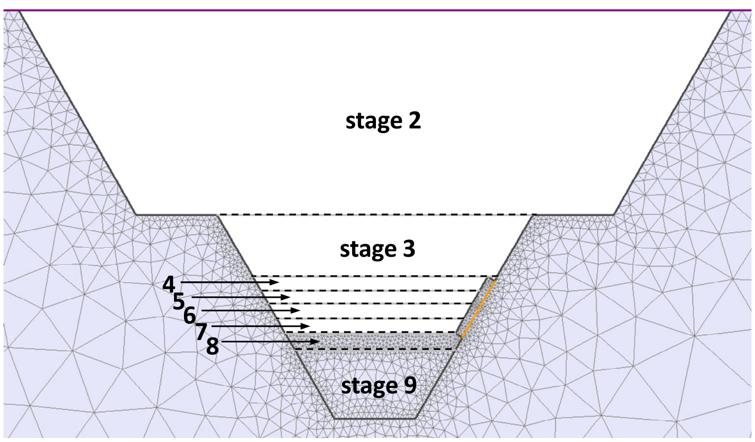

Figure 6 Case 2 with multiple stages along the slab showing the pit floor at stage 7

The model specifications including the type and number of elements, the convergence parameters including the tolerance and number of iterations, material and joint properties as well as model boundaries were kept the same. The ratio of maximum horizontal stress to vertical stress was set to 2 in these analyses.

Figure 7 shows the distributions of shear stress along the joint at different stages. Results demonstrate that at stages 2 and 3, the sense of shear stress is negative (upward relative slab motion) and is approximately constant throughout the joint. At stage 4, the magnitudes of shear stress along the portion of the joint associated with the unloaded portion of the slab drop to lower negative values. The shear stress reversal first occurs at the top of the joint at stage 5 where half of the slab is exposed. This figure clearly shows that as more of the slab is exposed due to the progressive downward advancement of the pit floor, the sense of shear stress along the top to the bottom of the joint progressively becomes positive. Moreover, as the pit floor passes the slab, the location at which the joint is subjected to the shear stress reversal (change in the sense of shear stress) moves downwards from the top to the bottom of the joint. For example, the shear stress reversal occurs in the middle of the joint at stage 7, while it occurs approximately at three quarters from the top of the joint at stages 8 and 9, when the slab is fully exposed. It is believed that this process can progressively degrade the shear strength of bedding surfaces.

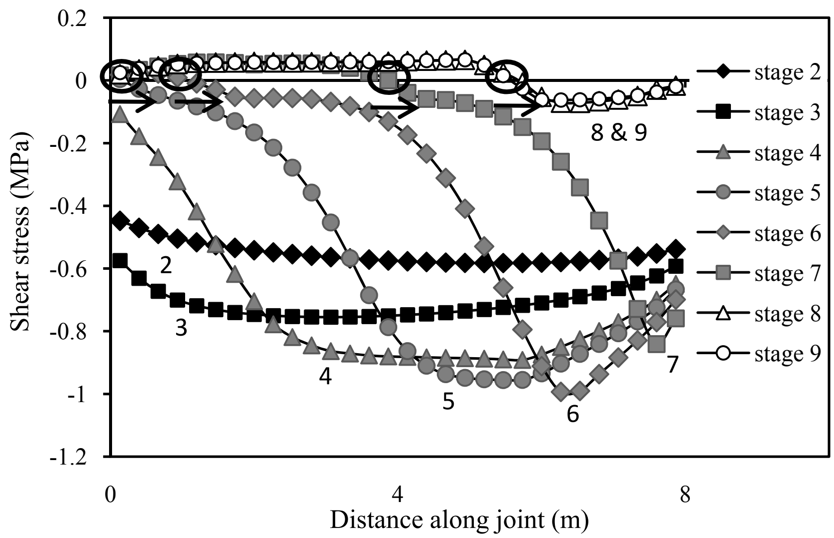

Figure 7 Shear stresses along the joint at different stages

Figure 8 displays the distributions of shear displacement along the joint at different stages. This figure indicates that the shear displacements are negative at all the stages. Initially the slab moves upward from stage 2 to 4. At stage 5, where half of the slab is exposed, the upper portion of the slab begins to slide downward. At this stage when this portion reverses its shear direction, the remaining part of the slab continues to move upward. With subsequent stages, a larger portion in the upper part of the slab reverses its shear direction and begins downward slip and a smaller portion in the lower part of the slab moves upward. After all the excavation stages, the joint still has a net upward displacement everywhere. This means that the slab started to move upward along the joint due to the elastic rebound from stage 2 to 4, and then progressively move downward from stage 5 to 9 due to the weight of the slab. However, even at stage 9, the slab has not yet returned to the position from which it had started to move upward at stage 2. The elastic-perfectly plastic joint has a ‘memory’ of its stress and displacement history associated with the pit floor being mined past the slab position.

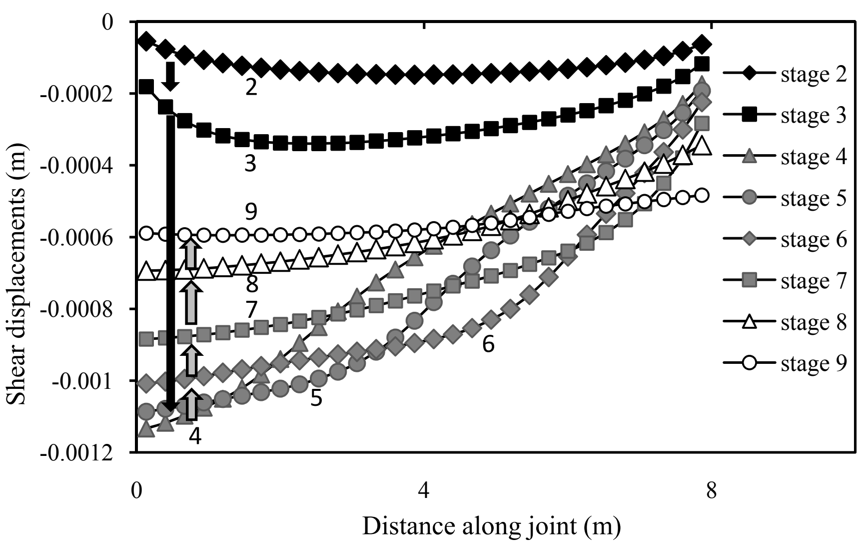

Figure 8 Shear displacements along the joint at different stages

Further insight can be gained by examining the results at specific points in the joint as the pit floor approaches and passes by. The downward black arrows in Figure 8 indicate that the shear displacement magnitudes at the top of the joint increase from stage 2 to stage 4. The shear displacements reach their maximum values at stage 4 where the pit floor has passed this location. The shear displacement magnitudes decrease to lower negative values from stages 5 to 9 as shown with upward grey arrows. A similar process can be observed for different locations along the joint. Figure 9 shows graphically the positions of shear stress or displacement reversals relative to pit floor levels at different stages.

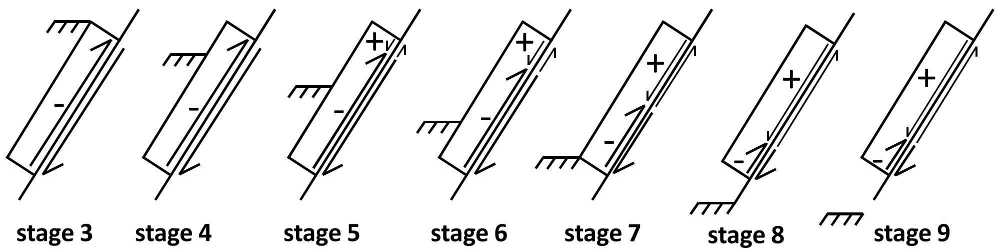

Figure 9 Shear stress or displacement reversal along the joint for different pit floor locations

The modeling results (shear reversals) shown in Figure 7 to Figure 9 suggest that shear strength degradation occurs during the excavation stages where the pit floor approaches and passes along the slab. A finite element analysis using elastic-perfectly plastic joint elements, however, cannot automatically simulate the process of shear strength degradation (fracture growth) caused by the shear stress and displacement reversals along the bedding surfaces. This shear strength degradation hypothesis should be validated by the use of a discrete element or a hybrid finite/discrete element code, which is beyond the scope of this paper.

The stress relief due to the unloading process is also believed to cause overstressing and yielding along the bedding planes. This conclusion was further explored by determining the cumulative and current numbers of yielded joint elements as well as the global factors of safety for slab slip at different stages in the numerical model. For determining the current number of yielded joint elements at a given stage, the factor of safety of each of the elements was calculated. The number of yielded joint elements at a current stage is then equal to the number of elements for which their factor of safety is calculated to be 1. The comparison between the current and cumulative numbers of yielded joint elements at different stages is shown in Figure 10.

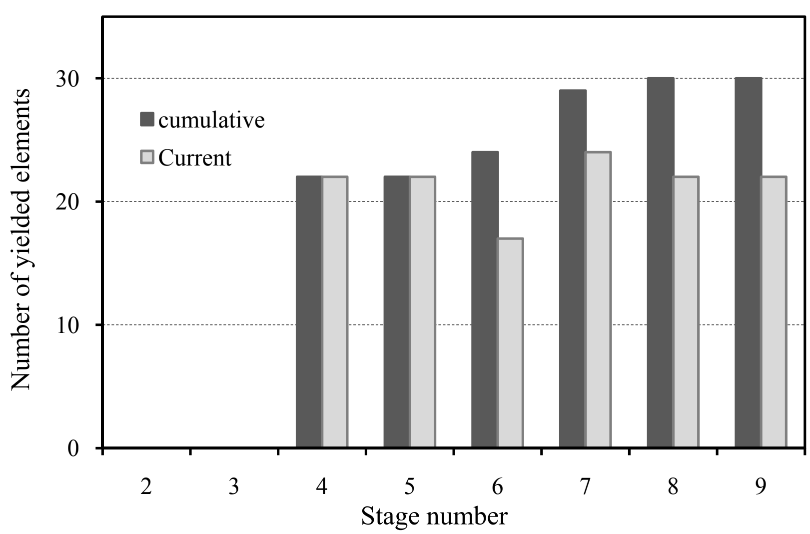

Figure 10 Cumulative and current numbers of yielded joint elements at different stages

As shown in Figure 10, at stages 2 and 3, none of the joint elements have yielded. A significant increase in the number of yielded elements at stage 4 highlights the importance of this stage on the unloading-induced shear strength degradation. This figure also shows that the cumulative number of yielded joint elements increases as the pit floor progresses to deeper levels where yielding occurs through all the elements at stages 8 and 9. The number of yielded joint elements at a current stage, however, indicates the highest amount of yielding occurs at stage 7 when the slab is partially exposed.

The results shown in Figure 10 answer the question that arose in Section 3. Previously, it was mentioned that yielding occured through all the joint elements in the last stage of Case 3 but the model converged and the calculated factor of safety was greater than unity. Figure 10 reveals that all the joint elements cumulatively yield at stages 8 and 9. The number of yielded joint elements that the software calculates and delivers to users is in fact the cumulative number of yielded joint elements. However, the software's stability analysis with the elastic-perfectly plastic joint boundary is based on the current status of the shear stresses acting on joint elements relative to the joint shear strength. The current number of yielded joint elements shown in Figure 10 indicates that only 20 out of 30 joint elements have yielded at stages 8 and 9 and hence the calculated global factor of safety is greater than unity.

Tracking the current and cumulative numbers and locations of yielded joint elements provides insight into the rebound-induced shear strength degradation of bedding surfaces. The first series of illustrations in Figure 11 show the yielded zones at a current stage. This figure indicates the importance of stage 4 (when the first part of the slab is exposed) on the shear strength degradation. It also shows that the largest zone of yielding occurs at stage 7. Diederichs et al. (2004) showed that the yielded zones resulting from changes in the stresses are indicative of crack propagation and its consequent strength degradation of rocks. They first modeled a sample with a discontinuity element as a crack tip with Mohr-Coulomb strength criterion. The stresses were then incrementally increased and rotated in different stages. This resulted in tensile rupture at the crack tip. Through different stages, the yielded finite element zones (ruptured zones) were replaced incrementally with joint elements, to simulate crack extension. A similar explanation can be used for the second series of illustrations in Figure 11. The cumulative yielded zones are indicative of progressive shear strength degradation that starts from the upper portion and progresses to the bottom of the joint as the pit floor approaches and passes the slab.

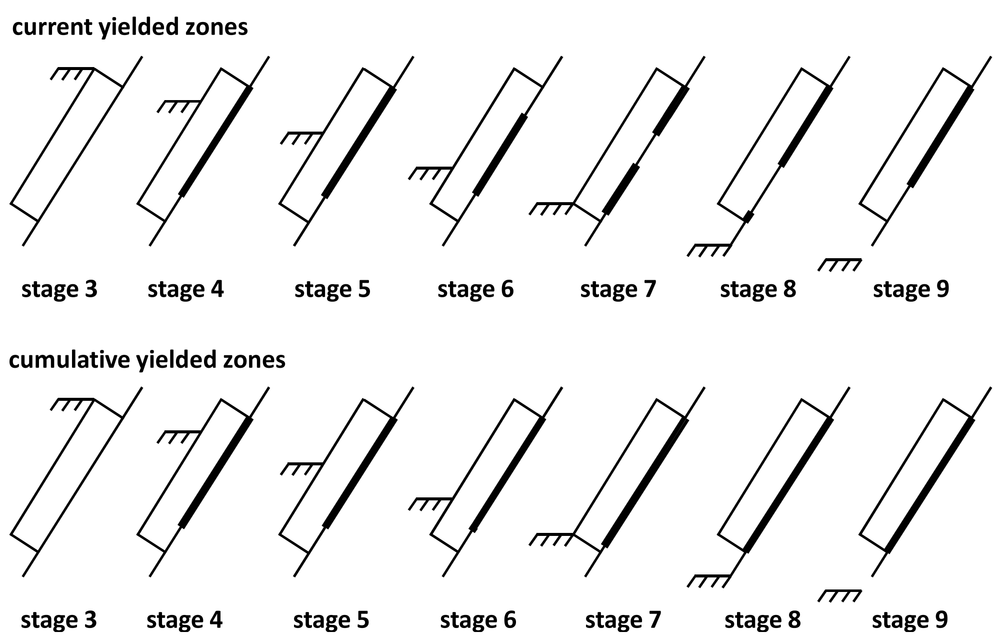

Figure 11 Current and cumulative yielded zones along the elastic-plastic joint at different stages

Further analyses were carried out to assess the influence of stress ratio on the unloading-induced shear strength degradation. For this purpose, the global factor of safety for slab slip was calculated at different stages for different values of in plane stress ratio (k = 1, 2 and 3) using Equation 2. Figure 12 suggests that the amount of shear strength degradation increases with increasing stress ratio from 1 to 3. It also indicates that the global factor of safety reaches its lowest values at stages 4 and 5 for different values of stress ratio (global factor of safety very close to 1 at stages 4 and 5 when $k = 3$) and becomes comparable to the limit equilibrium factor of safety obtained from Equation 1 at stages 8 and 9, when the slab is fully exposed for different values of stress ratio. This result further explains the importance of the stages in which the slab is exposed by the pit floor on the shear strength degradation of bedding surfaces caused by the unloading and rebound processes.

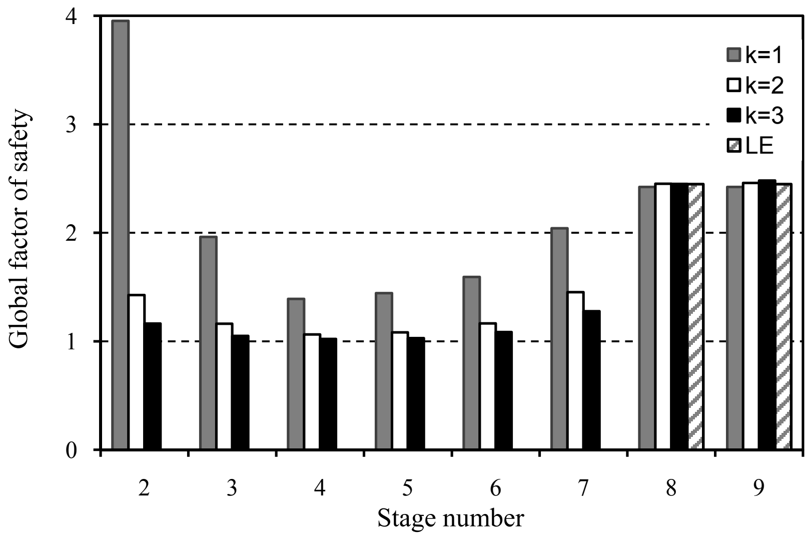

Figure 12 Factors of safety for slab slip at different stages

5 DISCUSSION AND CONCLUSION

The effect of surface excavation on the strength degradation of the remaining rock mass in open pit environments has not been widely acknowledged. Few examples in the literature examine the influence of unloading and elastic rebound on the strength degradation as well as the stability of natural or man-made slopes. In this study, the finite element program Phase2 was used to assess this effect on progressive shear strength degradation of bedding surfaces. For this purpose a planar footwall slab, typical of a stability concern at mountainous surface coal mines, was modeled with different excavation stages and pit depths. The main conclusions can be summarized as follows:

- The distributions of shear stress, normal stress, and shear displacement along the joint in the single stage model (Case 1) are different from those in the last excavation stage of Cases 2 and 3 in which the footwall slope is gradually exposed through multiple excavation stages.
- The finite element global factor of safety for slab slip in Case 1 obtained from Equation 2 is close to those from the last stage of Cases 2 and 3, as well as to the limit equilibrium factor of safety obtained from Equation 1.
- The cumulative number of yielded joint elements in Case 1 is different from that in Cases 2 and 3. This number increases with increasing pit depth.

To better understand the effect of excavation unloading and the consequent elastic rebound on shear strength degradation of bedding surfaces, Case 2 was remodelled with multiple stages along the footwall slab. The shear stress and displacement distributions along the joint at different stages were compared. The shear stress and displacement reversals seen along the joint boundary support the hypothesis of progressive shear strength degradation from the top to the bottom of joint during the stages that the pit floor approaches and passes the footwall slab.

The numbers and locations of cumulative and current yielded joint elements caused by stress relief due to excavation unloading at different stages were also obtained. The results suggest that the largest degree of shear strength degradation occurs when the footwall slab is being passed by the pit floor. The locations of yielded joint elements indicate that the shear strength progressively degrades from the top to the bottom of the joint as the pit floor approaches and passes the footwall slab to deeper levels. The global factors of safety for slab slip at different stages for different values of stress ratio were also determined. The lower factors of safety obtained at stages 4, 5 and 6 further supports the higher degree of shear strength degradation at these stages rather than when the slab is fully undercut. Moreover, the shear strength degradation at these stages increases (global factor of safety decreases) with increasing stress ratio from 1 to 3.

Bedding planes and joints often exhibit brittle or strain softening behaviour where there is a sudden loss of strength when the stresses reach the peak strength values. The current version of Phase2 cannot simulate strength loss after peak for joint elements. However, one can manually simulate this process by reassigning lower strength properties to the joint elements between stages. If an elastic-brittle constitutive model could have been used for the joint elements, the shear strength of the yielded joint elements would have probably dropped to their residual values at stage 4 when the shear stress exceeded the peak joint shear strength. This would have resulted in redistribution of stresses adjacent to the joint boundary and further yielding of other joint elements. For subsequent excavation stages, if yielding had occurred through all the joint elements, the factor of safety for slab slip would have been 1.0 and when the slab was finally undercut at stage 8 the model would not have converged, indicating slab failure. This model behaviour would have better simulated the excavation-dependent progressive shear strength degradation of bedding surfaces. This phenomenon should be considered when assessing the stability of footwall slopes that are exposed by mining activities.

REFERENCES

Deng J.H., Lee C.F. & Ge X.R. 2001. Characterization of the disturbed zone in a large rock excavation for the Three Gorges Project. *Can. Geotech. J.*, **38**: 95-106.

Diederichs M.S., Kaiser P.K. & Eberhardt E. 2004. Damage initiation and propagation in hard rock during tunnelling and the influence of near-face stress rotation. *Int. J. Rock Mech. and Min. Sci.*, **41**: 785-812.

Eberhardt E. 2001. Numerical modelling of three-dimension stress rotation ahead of an advancing tunnel face. *Int. J. Rock Mech. and Min. Sci.*, **38**: 499-518.

Eberhardt E., Stead D. & Coggan J.S. 2004. Numerical analysis of initiation and progressive failure in natural rock slopes-the 1991 Randa rockslide. *Int. J. Rock Mech. and Min. Sci.*, **41**: 69-87.

Goodman R.E. & Kieffer D.S. 2000. Behavior of rock in slopes. *J. Geotech. and Geoenvir. Engrg.*, **126** (8): 675- 684.

Hoek E. & Bray J.W. 1981. *Rock Slope Engineering, 3rd edition*. IMM, E&FN Spon, 358 p.

Imrie A.S. 1991. Stress-induced response from both natural and construction-related processes in the deepening of the Peace River valley, B.C., *Can. Geotech. J.*, **28**: 719-728.

Kaiser P.K., Yazici S. & Maloney S. 2001. Mining-induced stress change and consequences of stress path on excavation stability - a case study. *Int. J. Rock Mech. and Min. Sci.*, **38**: 167-180.

Krahn J. 2003. The 2001 R.M. Hardy Lecture: The limits of limit equilibrium analyses. *Can. Geotech. J.*, **40**: 643-660.

Matheson D.S. &Thomson S. 1973. Geological implications of valley rebound. *Can. J. Earth Sci.*, **10**: 961-978.

Panthi K.K. & Nilsen B. 2006. Numerical analysis of stresses and displacements for the Tafjord slide, Norway. *Bull. Eng. Geol. Environ.*, **65**: 57-63.

Rocscience. 2007. Phase2 v 6.0, Finite element analysis for excavations and slopes, Available from http://www.rocscience.com/products/Phase.asp.

Sheng Q., Yue Z.Q., Lee C.F., Tham L.G. & Zhou H. 2002. Estimating the excavation damaged zone in the permanent shiplock slopes of the Three Gorges Project, China. *Int. J. Rock Mech. and Min. Sci.*, **39**: 165-184.

Sheorey, P.R. 1994. A theory for in situ stresses in isotropic and transversely isotropic rock. *Int. J. Rock Mech. and Min. Sci. and Geomech. Abs.*, **31**: 23-34.

Stead D. & Eberhardt E. 1997. Development in the analysis of footwall slopes in surface coal mining. *Engineering Geology*, **46**: 41-61.